Eur. Phys. J. B **46**, 529–534 (2005)
DOI: 10.1140/epjb/e2005-00285-1

THE EUROPEAN PHYSICAL JOURNAL B

Simulation of the delamination of thin films

S. Scarle[a], C.P. Ewels[†], and M.I. Heggie

Chemistry Department, School of Life Sciences, University of Sussex, Falmer, Brighton, BN7 1QJ, UK

Received 12 January 2005 / Received in final form 29 March 2005
Published online 7 September 2005 –

Abstract. We simulate thin film delamination using a lattice springs model. We use this model to construct a phase diagram of different delamination behaviours, produced by varying the compression of the film and also the radius to which local relaxation is allowed to take place about failing bonds. From this we see a progression from laminar and linear behaviours to radial and rounded features as compressive stress is increased. Sinusoidal *telephone cord* behaviour occurs only at a small range of fairly low stresses, and thin films.

PACS. 68.55.-a Thin film structure and morphology – 46.32.+x Static buckling and instability – 47.54.+r Pattern selection; pattern formation

1 Introduction

Design and applications of thin films are often limited by failure at the film-substrate interface, since the *inter*-plane bonding is normally far weaker than the *intra*-plane bonding. Films can delaminate and then buckle up from their substrates when placed under a compressive stress. Once begun it can lead to catastrophic failure, as delamination tends to self-catalyze. Such a process can also be catalyzed through external effects such as moisture intercalation between film and substrate.

The sinusoid is one of a family of delamination behaviours [1–7]: dendritic buckling and cracking, unstable growth of straight sided delamination [8], flower cracking, bulge deformation (e.g. paint bubbles), string of beads [9], rippling front and island formation (tensile strain). All of these modes can be observed at many different length scales, and in many different materials. For a general review see Gioia and Ortiz [6].

Thin film delamination can be difficult to probe experimentally, due to the short time frames under which delamination often occurs. This makes it difficult to determine even basic information about film stress: for example, if two films exhibit different delamination behaviour, which one was under the highest internal stress? This can be overcome in some cases by studying slow delamination processes using a surface probe technique such as atomic force microscopy (AFM). Indeed there have been some very successful studies of dynamic delamination processes studied in this way [10–14]. However such studies are still limited in their ability to examine film delamination as a function of various film parameters in a way that theoretical studies can.

For this reason we have developed a new lattice spring model for modelling thin film delamination. We examine the change in delamination behaviour as a function of various parameters including film strain, thickness and relaxation radius. This allows us to construct phase diagrams of delamination behaviour.

In addition since we consider delamination numerically via a discrete grid of pseudo-atoms, it is possible to vary film and substrate properties at a local level. This allows simulation of effects such as stress corrosion cracking, whereby properties of the film near to the failure vary from that of the rest of the bulk film.

In the following sections we first summarize the literature on film delamination. We then describe our lattice spring model, and go on to describe the different *phases* of delamination behaviour observed as we altered various system parameters such as compressive strain, film relaxation range, and film thickness. Finally we draw some conclusions from these results.

2 Background

Sinusoidal or telephone cord blisters have been observed in many systems [6,9,15]. Originally it was thought these patterns were due to an anisotropic component of the compression, but this was experimentally found not to be the case [16], as confirmed theoretically with the lattice simulation of Crosby and Bradley [17]. Properties of the material in question can be obtained from measurements performed on these structures [18].

[a] e-mail: s.scarle@sheffield.ac.uk
Current address: Computer Sciences, University of Sheffield, Regent Court, 211 Portobello Street, Sheffield, S1 4DP, UK
[†] *Current address*: Laboratoire de Physique des Solides, Université Paris-Sud, Bâtiment 510, 91405 Orsay Cedex, France

In some cases although the delamination appears sinusoidal (*telephone cord*), it is actually a concatenation of arcs of circles [6]. Ortiz and Gioia [19] predicted a transition from straight sided to telephone cord morphologies at a critical mismatch strain, using a formulation of the energy of the film using an eikonal approximation to the von Kámán theory of moderate deflections of a plate (a continuum mechanics approach). They showed that the boundary of a blister has a critical radius of curvature ρ_c. If sections of the boundary have radii of curvature below ρ_c they are stable, if they are higher than ρ_c they will spontaneously delaminate until they reach ρ_c. In extended blisters, this can only be achieved by having the boundary form circular arcs separated by cusps, giving the telephone cord shape. This was experimentally corroborated by Thouless [20], who drilled a line of holes in a Al-mica composite. This showed that the straight edged blister, formed originally, changed to a telephone cord as the material cooled. This transformation occurred by the blister edge moving out.

Since telephone cords usually grow at the delamination tip, this lateral delamination cannot easily be separated from the forward motion of the tip, and so the blister can appear to propagate in a meandering fashion. This is corroborated by theoretical work which shows that from a continuum mechanics view-point the string of beads (another form of delamination, whereby the film lifts in a line of equal height mounds) and the sinusoidal form both appear as aspects of the same behaviour, with merely a phase change in the respective solutions [21].

An important process in thin film delamination is stress corrosion cracking, whereby a solvent such as water enters the interface between film and substrate through a break in the film, weakening nearby bonds and causing the stress to release the film from the substrate. This has been observed with, for example, BN films on silicon [22]. As bonds in the area fail the water is able to percolate further beneath the film. Failure by this mechanism demonstrates distinctive delamination behaviour. Notably, delamination occurs in failed BN on Si films both at the propagating front and in isolated bubbles *ahead* of this front, suggesting water moving ahead of the delamination [22].

As well as delamination of surface coatings, surface layers of bulk material can also delaminate, for example through accumulation of defects such as occurs under hydrogen ion bombardment in silicon. In this case the process, known as the Smart-Cut$^{\mathrm{TM}}$ process [23,24], leaves an atomically smooth Si surface after delamination. Hydrogen platelets are formed parallel to the surface which expand and at high hydrogen concentration these platelets are able to reach a critical size. Internal pressure of H_2 molecules leads to a blistering of the surface [25–27]. If a silicon wafer after implantation is bonded to another and then annealed, this blistering turns into delamination, producing a uniform layer of silicon on top of the newly bonded crystal [25,23,24]. The technology of Smart-Cut is well known, but the underlying physics and chemistry (i.e. details of structure of micro-cracks and microscopic phenomena at the platelet and the resulting blistering and delamination) are not yet well understood.

3 Model

Previous work in the literature has used a number of techniques including Finite Element [8,29] and continuum elasticity related techniques [6,7,28]. 2D continuum approaches require the assumption that the film is of ideal thickness (i.e. infinitesimal), and so cannot talk about cases where the film thickness and features of the delamination are on the same length scale. Such problems instead require 3D continuum elasticity [7]. A further problem caused by having lengths tending to zero is that it is unclear as to how one should define a small length cutoff. This makes the failure mechanism difficult to describe when delamination takes place. To circumvent this problem, and to increase model flexibility, we take a lattice spring approach [17].

Our model takes an hexagonal close packed [HCP] lattice of pseudo-atoms. It should be noted that we are not taking a genuinely atomic scale view, as the effects of *thin film* delamination can be observed at almost any length scale. Our elements are small volumes of the surface. These are bonded to all nine of their HCP neighbours by Hookean springs,

$$E_{ij} = K[T_i, T_j](x_{ij} - n_{ij})^2 \tag{1}$$

where E_{ij} = energy due to the *bond* between elements i and j, $K[T_i, T_j]$ = spring coefficient of a bond between element types T_i and T_j, x_{ij} = separation between i and j, n_{ij} = ideal separation of i and j. We can choose the number of layers on the surface, typically using one fixed substrate layer and two film layers, which are allowed to relax.

Some given set of bonds are broken to start the simulation (i.e. their Ks are set to zero) and all positions of elements out to Nth nearest neighbour of the broken bonds within the film layers are relaxed. This value N we call the relaxation radius of the simulation. The most strained whilst stretched bond after this relaxation is then broken, that is the one with maximal E_{ij} given that $x_{ij} - n_{ij} > 0$. The elements out to Nth nearest neighbour of this broken bond are then relaxed, using the L-BFGS-B FORTRAN subroutine [30]. This process is then iterated.

The L-BFGS-B FORTRAN subroutine is a standard minimization routine implementing a limited-memory quasi-Newton code for large-scale bound-constrained or unconstrained optimization and is available widely on the net [31].

Our choice of energy model is a compromise between something that reasonably reflects the underlying film dynamics while at the same time allowing us to perform a great many calculations on large systems in reasonable times. Our intention is to produce a series of events in correct temporal order, not perform a physically accurate kinetic simulation, so only relative energies and behavioural

ordering of the structures is important, not their quantitative/absolute values. Even if we might expect occasional deviation from this ordering in real physical systems due to statistical distribution of behaviour, the structure after hundreds of events will not be seriously modified, or at the very least not qualitatively modified.

As stated above our approach allows for great flexibility in what can be modelled. A discretized grid allows us to vary bond strengths via the chosen spring constants, as well as, for example, randomization of starting bond lengths. This allows simulation of a number of physical thin film properties such as mixed composition films. Previous attempts to incorporate variation in film response have been limited, for example using fuzzy logic to describe the interaction between different materials parameters [29].

The relaxation radius needs further discussion. Although originally introduced to reduce calculation time compared to a full film relaxation, it can be viewed as a ratio of time scales between the process of bond breaking and the resulting relaxation. Thus it is primarily a numerical representation of the physical situation of stress-corrosion cracking, where the delamination front and solvation front are coincident. In this case the cut-off radius corresponds to the diffusion length of the corroding species (e.g. atmospheric water) within the time between bond breaking events. For more detailed incorporation of stress-corrosion cracking, this model easily allows for alteration of the K values out to a higher radius about a failed bond. This second modification would simulate the solvation front preceding the delamination front. In this way dynamic, local variations in film properties can be incorporated during the lifetime of the simulation.

4 Results

The above model was run for a rhombohedral slab of material, with 300 elements along each side and three layers thick, i.e. one substrate layer (held fixed) and two movable thin-film layers. Giving a system of $300 \times 300 \times 3 = 270\,000$ elements. Only bonds between substrate and film were allowed to fail. The system had periodic boundary conditions within the plane. It was initiated by breaking all bonds to the substrate for a single central element. Initially all elements were set at the ideal positions for the substrate lattice spacing. We re-emphasize that this is not intended as an atomic scale model and that the separate elements in the simulation are meant to represent mesoscale volumes of film rather than individual atoms. For this reason the length scale on the diagrams for Table 1 are arbitrary.

A phase diagram (Fig. 1) was produced by varying both the relaxation radius N (varied from one to twenty elements), and the compressive stress applied to the film. This stress was measured by setting the ideal element spacing of the film elements to be a given percentage higher than that of the substrate elements, and was varied from a 1% increase up to 30%, in 1% steps. The ideal separation between film and substrate elements was taken as the average of the ideal element spacings for the film and substrate. The resulting phases are described in Table 1, and in the following paragraph.

In general we observe a number of trends from our phase diagram. At low applied stresses the film tends to delaminate to a uniform height and little buckling is observed, however we do observe ridges, cords and other linear behaviour, phases 3 and 4. In a limited number of cases we observe a flat behaviour, phase 2, whereby the film produces a straight line delamination front along which bonds sequentially fail, moving the front forward until the whole film has relaxed to an equal height.

At higher stresses these are replaced with more localized radial features such as bubbles and blisters. These start out as small lumps at the centre of hexagonal raised areas of flat delamination (hexagonal cells, phase 5), and as the stress increases go on to form rafts of blisters (phase 6). The size of the blisters increases with relaxation radius. At very low relaxation radius we also get occasions where no delamination takes place, phase 0, or in an extremely low number of cases where it is unclear as to the behaviour, phase 1.

Although the hexagonal nature notable in phases 4 and 5 is a reflection of the underlying symmetry of the elements and their bonding, the basic form of these modes is likely to be close to the actual physical manifestations of these phases. Namely, we suspect that the hexagonal line (phase 4) may represent a more dendritic mode of delamination. In our case the model is restricted to breaking a single bond at a time, but the regular alternation in direction of the hexagonal line front suggests an unstable delamination front. In a more finely discretized system with multiple simultaneous bond failures such crack lines could easily bifurcate. The hexagonal nature may also be retained due to basic geometric arguments. Interestingly, the stress at which the hexagonal cell type of behaviour both begins and gives way to the bubble raft form does not appear to vary with relaxation radius.

This progression from linear to more radial features is observed experimentally, even in the case of a uniaxial stress [12] where in a Nickel film/polycarbonate substrate system, linear wrinkles perpendicular to the axis change to roughly sinusoidal ones as the stress increases. Similarly, Audoly et al. [33] have shown a similar development with biaxial stress, using both experimental and Föppel-von Kármán theoretical analysis.

However, in related work [13] with 304L stainless steel on polycarbonate, such a transformation is an aging process of the linear wrinkles, so as to optimally release stress in the transverse direction.

We also ran simulations with thicker films, by increasing the number of film layers from two up to nine. Sparser phase diagrams were produced for these further runs, and showed little change in the overall form of the phase diagram, however the regions of no and unclear delamination behaviour continued to higher relaxation radii, in proportion with the increased thickness of the film. There was no obvious change in the length scale of the observed patterns. However, the size of the bubbles in their rafts

Table 1. Table of the colours assigned to each phase shown in the Phase Diagram. Intermediate colours represent intermediate phases. Images of the delaminating film such as these were produced for each point on the phase diagram using the PovRay [34] ray-trace program and classified manually for the phase diagram. x and y axes of the images are approximately 185 elements long.

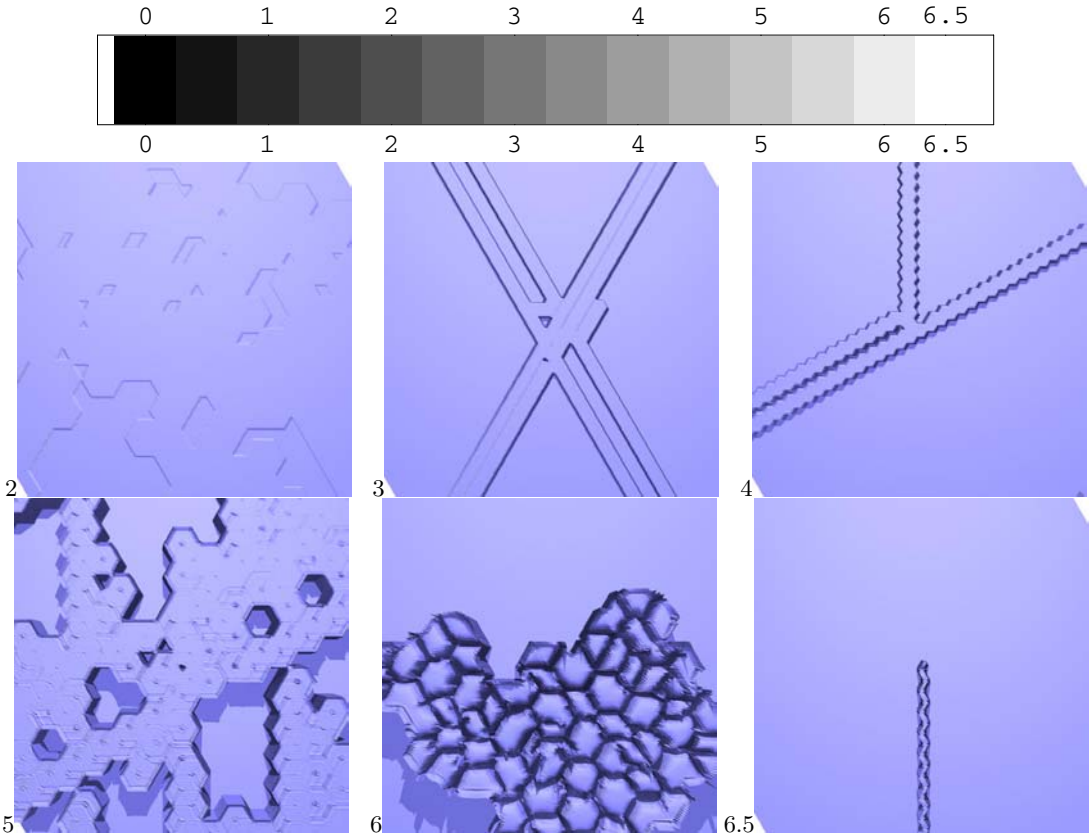

Phase/Colour	Name	Description
0	none	no delamination
1	unclear	unclear as to which behaviour
2	Flat	to a uniform height
3	Line	as 2 but with linear features
4	Hexagonal Line	as 3 but with HCP features
5	Hexagonal Cells	lumps at the centre of hexagonal raised areas
6	Bubble raft	close mat of bubbles
6.5	Sinusoidal	... or telephone cord

decreases with the ratio of film thickness to relaxation radius.

The increased strain range for no delamination in thicker films is reasonable, since one effect of thickening the film is to make it more rigid. Multiple film layers are a way of effectively introducing an angular three body term to our two body spring model, since angular distortions in one layer will strain bonds in neighbouring layers (see Fig. 2). In addition the strain is dispersed more effectively, lowering the required extension of each individual bond.

There was also a slight decrease (2%) for the on set of the hexagonal and bubble raft behaviour as film thickness increased. This suggests weak correlation between film thickness and delamination behaviour, consistent with links between sinusoidal delamination and film thickness observed by Crosby et al. [17].

We only observe telephone cord behaviour (phase 6.5) in a very small range of stresses, consistent with work of Crosby and Bradley [17]. We also only observe such behaviour when using a small relaxation radius. This corresponds either to rapid rate delamination, or stress corrosion cracking regimes where only nearby bonds are weakened. Finally, we only observed telephone cord behaviour in the thinnest films, although there is a possibility it is not observed in the thicker films due to the courser grain grids used.

Isotropic strain is known to lead to sinusoidal behaviour in crack propagation [32], and the mechanism in thin film delamination should be the same. An arch

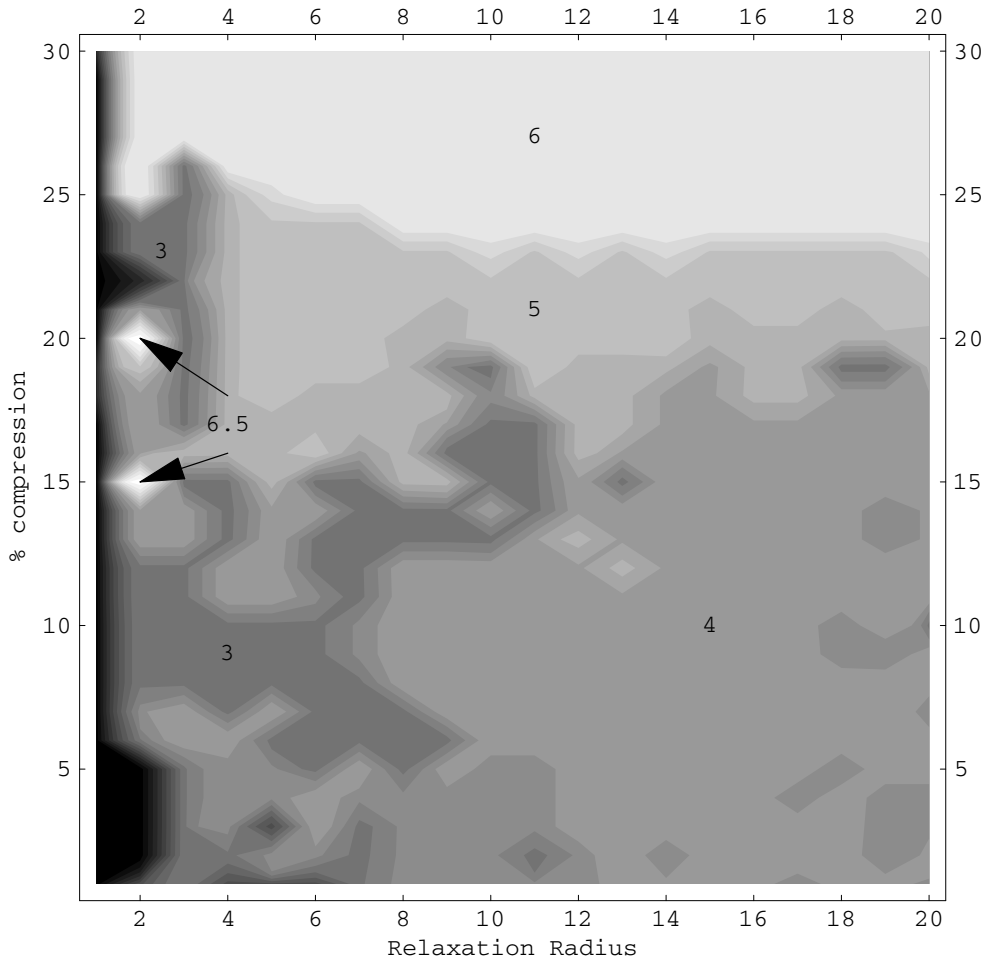

Fig. 1. Phase diagram for delamination of a 2 layer thick film on a fixed substrate. The legend and explanation of phases are shown in table 1.

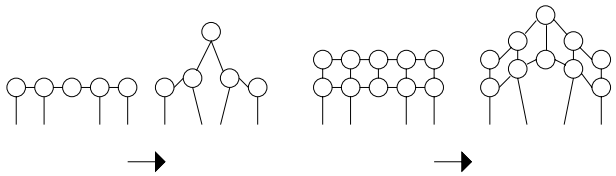

Fig. 2. Multiple film layers effectively add a 3-body term to our potential, preventing film stress relief through massive angular distortion (a), since in a multi-layer film this compresses the bonds between the layers (b).

structure reduces stress, but it only does so perpendicular to the direction it faces. To relieve maximal stress it must change direction during propagation to relieve orthogonal components of stress. This should lead to circular rotational behaviour of the propagating front, however after rotating 180° it starts to encounter regions of film already relaxed by earlier sections of the delamination. Thus there will be a driving force to reverse the direction of rotation. The result of this rotating and switching is that the delamination front propagates via a series of semicircles. Given the other telephone cord models summarized above, it seems possible that there maybe different mechanisms leading to visually similar delamination modes.

The fact that we have a limited relaxation radius and break bonds one at a time restricts the ability of the film to relax and delaminate. At extremely high stresses this results in bubble type behaviour when in fact we may expect the whole film to spontaneously delaminate from the surface. At low stresses where film response can occur over relatively long time scales, we might expect some increased buckling due to additional strain from the surrounding material.

5 Conclusion

Using a simple lattice model, we have studied the failure of compressively strained thin films on solid substrates. Our simulations reproduce a number of different phenomenologies of thin-film delamination. This includes a sinusoidal form, but only in a limited region as expected.

At low stresses we observe uniform delamination, with various linear features. As stress increases more radial features are obtained (hexagonal cells, bubble rafts). There is

no change in the stress of crossover between these regimes with increasing relaxation radius, but there is a slight decrease with increasing film thickness.

This puts us in broad agreement with a number of pieces of both experimental and theoretical work [10,12,33] which show a commensurate progression from linear to more radial buckling with an increasing stress.

In principle our approach is extremely general and should be applicable to a range of problems at different length scales, for example paint blistering, compressed deformation bands in porous sandstones and perhaps even tectonic plate interaction. It would now be simple to incorporate additional features such as variable K and bond lengths, allowing simulation of heterogeneous films and stress corrosion cracking.

We would like to thank the Sussex High Performance Computer Initiative [SHPCI] for the use of the BFG computer system, and we acknowledge funding support from the European Grant programme Transdiam. C. Ewels acknowledges the EU Marie Curie Individual Research Fellowship Scheme contract MCFI-2002-01436 for financial support. We acknowledge stimulating discussion with the group of K. Zellama at the Université de Picardie which led to this work. The FORTRAN source code for this program is available from the authors via `S.Scarle@sheffield.ac.uk`.

References

1. S.P. Lacour, S. Wagner, Appl. Phys. Lett. **82**, 2404 (2003)
2. N. Bowden, S. Brittain, A. G. Evans, J. W. Hutchinson, G.W. Whitesides, Nature (London) **393**, 146 (1998)
3. G. Lazar, M. Clin, S. Charvet, M. Therasse, C. Godet, K. Zellama, Diamond & Related Mat. **12**, 201 (2003)
4. R.C. White, S.S. Bhaia, M.C. Friedenberg, S.W. Meeks, G.M. Mate, Tribology **6**, 33 (1998)
5. G.A.J. Amaratunga, S.R.P. Silva, Appl. Phys. Lett. **68**, 2529 (1996)
6. G. Gioia, M. Ortiz, Adv. Appl. Mech. **33**, 119 (1997)
7. B. Audoly, J. Mech. & Phys. Solids **48**, 2315 (2000)
8. H. Jensen, I. Sheinman, Int. J. Fracture **110**, 371 (2001)
9. S.B. Iyer, K.S. Harshavardham, V. Kumar, Thin Solid Films **256**, 94 1995
10. C. Coupeau, Thin Solid Films, **406**, 190 (2002)
11. G. Binnig, C.F. Quate, C. Gerber, Phys. Rev. Lett. **56**, 930 (1986)
12. C. Coupeau, J.F. Naud, F. Cleymand, P. Goudeau, J. Grilhé, Thin Solid Films, **353**, 194 (1999)
13. F. Cleymand, C. Coupeau, J. Grilhé, Scripta Materialia **44**, 2623 (2001)
14. P. Besuelle, P. Baud, T.F. Wong, Pure Appl. Geophys. **160**, 851 (2003)
15. T. Zehnder, J. Balmer, W. Lüthy, H.P. Weber, Thin Solid Films **263**, 198 (1995)
16. K. Ogawa, T. Ohkoshi, T. Takeuchi, T. Mizoguchi, T. Masumoto, Jpn J. Appl. Phys. **25**, 695 (1986)
17. K.M. Crosby, R.M. Bradley, Phys. Rev. E **59**, R2542 (1999)
18. G. Gioia, M. Ortiz, Acta Mater. **46**, 169 (1998)
19. M. Ortiz, G. Gioia, J. Mech. Phys. Solids **42**, 531 (1994)
20. J.W. Hutchinson, M.D. Thouless, E.G. Liniger, Acta Metal. Mater. **40**, 295 (1992)
21. B. Audoly, Phys. Rev. Lett. **83**, 4124 (1999)
22. J. Möller, D. Reide, M. Bobeth, W. Pompe, Surf & Coatings Tech. **150**, 8 (2000)
23. M. Bruel, Nucl. Instr. Mech. B **108**, 313 (1995)
24. B. Aspar, M. Bruel, H. Moriceau, C. Maleville, T Poumeyrol, A.M. Papon, A. Claverie, G. Benassayag, A.J. Auberton-Herve, T. Barge, Microelec. Eng. **36**, 233 1997
25. M.K. Weldon, J. Vac. Sci. Tech. B **15**, 1065 (1997)
26. Q.Y. Tong, Appl. Phys. Lett. **70**, 1390 (1997)
27. L.J. Huang, Appl. Phys. Lett. **74**, 982 (1999)
28. P. Peyla, Phys. Rev. E **62**, R1501 (2000)
29. A. Muc, Int. J. Fatigue **24**, 419 (2002)
30. C. Zhu, R.H. Byrd, P. Lu, J. Nocedal, *L-BFGS-B - Fortran subroutine for large scale bound constrained optimization*, Northwestern University EECS Technical Report NAM12 (1995)
31. `http://www.ece.northwestern.edu/~nocedal/lbfgsb.html`
32. B. Coterell, J.R. Rice, Int. J. Fract. **16** 155 (1980)
33. B. Audoly, B. Roman, A. Pocheau, Eur. Phys. J. B **27**, 7 (2002)
34. `http://www.povray.org`